Measurement of the absolute gamma-ray emission intensities from the decay of ^{103}Pd

Jonathan Riffaud, Marie-Christine Lépy, Philippe Cassette, Margot Corbel, Mark Kellett, Valérie Lourenço

▶ **To cite this version:**

Jonathan Riffaud, Marie-Christine Lépy, Philippe Cassette, Margot Corbel, Mark Kellett, et al.. Measurement of the absolute gamma-ray emission intensities from the decay of ^{103}Pd. Applied Radiation and Isotopes, 2021, 167, pp.109298. 10.1016/j.apradiso.2020.109298 . cea-03044305

HAL Id: cea-03044305
https://cea.hal.science/cea-03044305

Submitted on 8 Dec 2020

HAL is a multi-disciplinary open access archive for the deposit and dissemination of scientific research documents, whether they are published or not. The documents may come from teaching and research institutions in France or abroad, or from public or private research centers.

L'archive ouverte pluridisciplinaire **HAL**, est destinée au dépôt et à la diffusion de documents scientifiques de niveau recherche, publiés ou non, émanant des établissements d'enseignement et de recherche français ou étrangers, des laboratoires publics ou privés.

Measurement of the absolute gamma-ray emission intensities from the decay of ^{103}Pd

Authors: J. Riffaud, M.-C. Lépy*, P. Cassette, M. Corbel, M.A. Kellett, V. Lourenço,

Affiliation: CEA, LIST, Laboratoire National Henri Becquerel (LNE-LNHB), Bât. 602 PC 111, CEA-Saclay 91191 Gif-sur-Yvette Cedex, France

** Author for correspondence:* marie-christine.lepy@cea.fr

Abstract

Palladium-103 decays through electron capture to excited levels of ^{103}Rh, and especially to the 39.748-keV metastable state. A high activity palladium chloride solution was standardized by liquid scintillation, using the Triple-to-Double Coincidence Ratio method. The absolute photon emission intensities were determined by gamma-ray spectrometry using point sources prepared with the standard solution. Different detectors and measuring conditions were used to cross-reference the results. The most intense photon emission intensities are derived with about 1 % relative combined standard uncertainty.

Keywords: ^{103}Pd, gamma-ray spectrometry, liquid scintillation counting, TDCR, photon emission intensities, half-life.

Highlights:

- ^{103}Pd chloride solution standardized by liquid scintillation using the TDCR method.
- Absolute photon emission intensities obtained by gamma-ray spectrometry.
- Different detectors and measuring conditions to cross-reference the results.
- Most intense photon emission intensities obtained with about 1 % relative combined standard uncertainty.

Introduction

Palladium-103 is a radioisotope of interest in medical applications, used in brachytherapy implants for the treatment of prostate cancer. It decays through electron capture to excited levels of ^{103}Rh, and especially (99.99 %) to the 39.748 keV metastable state. The radioactive equilibrium between ^{103}Pd (half-life = 16.991 (19) d) and ^{103m}Rh (half-life = 56.114 (9) min) (De Frenne, 2009) is reached within about nine hours.

Palladium-103 was studied in the 1940s (Matthews and Pool (1947), Linder and Perlman (1948)), and details of the decay scheme were given by Mei *et al.* (1950), Rietjens *et al.* (1954), Avignon *et al.* (1955) and Saraf (1955). However, due to the poor energy resolution of scintillator-based detectors, only the principal features of the decay scheme were highlighted, especially the highly converted transition around 40 keV. The availability of germanium-based spectrometers with improved energy resolution, allowed more information to be determined. Nevertheless, difficulties in assigning spin and parity for two of the five levels populated in the decay of ^{103}Pd lead to conflicting results between Grunditz *et al.* (1969) and Zoller *et al.* (1969) decay schemes published the same year, or by Manthuruthil *et al.* (1968) in experiments conducted on ^{103}Ru (which also decays towards ^{103}Rh). A further study on ^{103}Rh by Avignone and Frey (1971) provided a documented decay scheme including detailed comment on spin and parity of the levels of ^{103}Rh, which was refined by Macias *et al.* (1976). A few more studies (Newton *et al.* (1978), Bazhenov *et al.* (1985), Berlyand *et al.* (2002), Popov *et al.* (2004)) provided some experimental photon emission intensities for the main lines. In a recent work dedicated to the study of internal conversion coefficients, Nica *et al.* (2018) discussed the multipolarity of the 39-keV transition which is studied in ^{103}Rh decay. Thus, up-to-now, due to the weak gamma emission intensities (< 0.1%), only those of the 357.45-keV emission were directly quantified, the others were obtained from measurements of relative values, or from

calculations taking into account the transition multipolarities and conversion coefficients. The decay scheme presented in Figure 1 is based on energy, spin and polarity of levels evaluated by De Frenne (2009).

In the present experiment, the mass activity of a ^{103}Pd chloride solution was determined by absolute liquid scintillation (LS) counting. In a previous article, Cassette *et al.* (2004) showed that the Triple-to-Double Coincidence Ratio (TDCR) method can be applied to standardize ^{103}Pd with a relative standard uncertainty around 0.3 %. The photon emission intensities were measured by gamma- and X-ray spectrometry using point sources prepared from the standardized solution. Different detectors and measuring conditions were used to cross-reference as much information as possible and to obtain the values of some low-intensity emissions. Due to the accurate knowledge of the sources' activities, absolute emission intensities could be derived. In addition, the half-life of ^{103}Pd was measured by gamma-ray spectrometry to provide further information on its decay scheme.

1. Source preparation

The ^{103}Pd supplied by NORDION (2019) consisted in palladium chloride in dilute ammonium hydroxide solution (1.10^{-3} mol.L^{-1}, pH ~ 10), with a nominal mass activity of 37 GBq.g^{-1}. It was necessary to dilute this solution both to change its chemical composition and to reach lower mass activities in order to perform the measurements. A solution around 10 MBq.g^{-1} was prepared in 3 mol.L^{-1} HCl containing 10 µg of stable rhodium per gram of solution, to ensure the chemical stability of ^{103m}Rh in equilibrium with ^{103}Pd. This diluted material also contained about 12 µg of stable palladium per gram, from the initial solution; these stable elements do not induce any significant self-attenuation in the sources. Source preparation and weighing were performed according to the procedures detailed by Lourenço and Bobin (2015).

For gamma-ray spectrometry measurements, six point sources were prepared with 9.8 mg to 19.5 mg of solution (100 kBq to 200 kBq per source) dried on 18-µm thick Mylar® sheet. The deposits were then covered with a thermo-sealable 12 $mg.cm^{-2}$ Terphane® foil and inserted in a plastic ring. During gamma-ray spectrometry measurements, the source side facing the detector is the thinnest one (18-µm thick Mylar®), as in the calibration configuration.

To standardize the ^{103}Pd solution by liquid scintillation counting, a dilution by a factor close to 20 (0.053189 (8)) was prepared in the same chemical medium to produce six LS sources. Each source contained about 5 kBq of ^{103}Pd in Ultima Gold® scintillator. About 100 µL of water were added to each source for stabilization purposes.

The impurity check performed on the initial solution did not reveal any gamma-emitting impurities. A complementary acquisition was performed one month after the emission intensity measurement, to benefit from the ^{103}Pd decay. Rhodium-101 (half-life = 3.30 (10) a) was detected with an activity relative to that of ^{103}Pd equal to 10^{-5} $Bq.Bq^{-1}$. Due to the ratio of half-lives, this value was about four times lower during the emission intensity determination and did not cause any significant disturbance.

2. Half-life measurements

The same palladium solution of known purity was used to determine the half-life of ^{103}Pd by gamma-ray spectrometry, using an aliquot of the diluted solution. The measurements were carried out for 50 days, on a high-purity germanium (HPGe) detector by recording the peak area corresponding to the 357.45-keV emission of ^{103}Pd. The duration of each measurement was 35 000 s live time, the statistical uncertainty in the peak area determination was less than 0.22 %. The relative dead time was low, from 1.29 % for the first measurement to 0.27 % for the last one. Thus, the corrective factor for decay during each acquisition was quite constant (about 1.0084). The resulting half-life value is 17.092 (57) d, derived from fitting an

exponential function to 121 experimental values, using the Marquardt-Levenberg algorithm, with a reduced chi-square of 18.189. However, among these, some discrepant values were noted: they correspond to acquisitions distortion induced by the automatic liquid nitrogen filling system (once a week). A second fit, excluding these nine experimental values and using the same fitting procedure, as shown in Figure 2, led to the half-life of 17.049 (16) d, with a reduced chi-square of 1.258. This value is compared to previously published data in Table 1. The present relative uncertainty is equivalent to those reported by Czock *et al.* (1975) and Vaninbroukx *et al.* (1981); in particular the present measurements were made using an HPGe- instead of an NaI-based spectrometer, hence more stable and with better energy resolution, which made it possible to select a specific gamma-ray line, thus avoiding any uncertainty due to possible impurities. A more detailed study of the ^{103}Pd half-life measurement is planned.

3. Absolute photon emission intensities

The absolute photon emission intensities were obtained by gamma-ray spectrometry using a solution whose mass activity was determined by liquid scintillation counting, using the Triple-to-Double Coincidence Ratio method.

3.1 TDCR measurement

The five LS sources were measured using the RCTD1 TDCR counter of the Laboratoire National Henri Becquerel (LNHB) (Cassette and Vatin, 1992). Each source was measured 10 times for 1 minute, allowing relative counting uncertainty of 6 10^{-4}. The detection efficiency was calculated using the model described by Cassette et *al.* (2004) with updated decay data parameters. The detection efficiencies, in double and triple coincidences, is a function of the

intrinsic light yield of the detector and can be calculated as a weighted sum of all individual efficiencies corresponding to the absorption of energy according to the possible atomic rearrangements following the gamma transition. This includes the absorption by the scintillator of the energy of the conversion electrons, but also of the energies of the associated Auger electrons and X-rays. For a large number of observed transitions, the ratio of triple to double detection efficiencies is assumed to be equal to the ratio of observed triple and double coincidences and this equality allows the determination of the intrinsic light yield of the scintillator, and thus the detection efficiency. The atomic rearrangement calculation is based on a simplified KLM model, *i.e.* without considering the L and M subshells and without distinction between the M and other outer shells. This assumption is justified by the low energy difference between the subshells (e.g. about 400 eV between the L1 and L3 energies) and also because the atomic rearrangements are coincident with the absorption of conversion electrons in the scintillator. The TDCR detection efficiency is obtained by calculating the normalized density function describing the energy spectrum absorbed by the LS-cocktail. This spectrum was calculated by considering all the possible de-excitation phenomena, calculating the associated energy deposition and probability and summing all these components. Evaluation of the energy transfer of the ionizing radiation to the LS-cocktail is obtained using the following assumptions:

i. The Auger and conversion electrons are totally absorbed by the cocktail,

ii. The XL emission is totally absorbed by the cocktail by photoelectric interaction,

iii. The XK emission interacts with the LS-cocktail by Compton and photoelectric effects.

The energy transferred to the cocktail is calculated using the Monte Carlo simulation code PENELOPE (Salvat, 2015). The calculation took into account the asymmetry of the photomultiplier tubes, by considering the three individual TDCR values (Broda *et al.*, 2007). The relative standard uncertainty due to the source dispersion was 0.13% and the global

uncertainty calculation (0.21%) was achieved by a global Monte Carlo simulation, following the recommendations of the supplement 1 of the Guide to the expression of uncertainty in measurement (GUM) (JCGM, 2008).

This Monte Carlo calculation used Gaussian fluctuations of the decay scheme parameters and the Birks factor (kB). The conversion of a gamma transition depends on the multipolarity of the transition, which is not well-established for ^{103m}Rh. From the previously reported X-ray intensities, the multipolarity is between E3 and E3+ 0.08% M4. The influence on the internal conversion coefficient values was calculated using the Bricc code (Kibédi *et al.*, 2005). From these values, we observed that the difference on conversion coefficients obtained within the two hypotheses on the multipolarity of the transition, are compatible with the associated claimed uncertainties. Thus, the values considered are the mean values of each data set with associated standard deviations. The fluctuations of the counting rates were taken into account by using the bootstrap method (Cassette et al., 2004).

The activity of the diluted solution was 503.8 (13) kBq.g^{-1} at the reference date of 19/12/2017, 12h00, UTC. Taking into account the dilution factor, this led to an activity concentration of the master solution of 9 472 (24) kBq.g^{-1} at the same reference date.

3.2 Gamma-ray spectrometry

Gamma-ray spectrometry and the calculation of the uncertainties are performed according to the procedures described in Lépy *et al*. (2015, 2016, 2018). First, the homogeneity of the six sources was checked by measuring the counting rate in the K X-ray region, for 1 000 seconds. For each source, the decay corrected rate per unit mass was determined. The relative standard uncertainty of each measurement ranged between 0.09 % and 0.13 %. The result for one of the six sources significantly deviated from the mean value (by 2.3 %) and was excluded. Finally, the relative standard deviation on the measurement on the five remaining sources was 0.21 %.

This value is considered as the uncertainty linked to the reproducibility of the sources, since only two of these were measured for determining the photon emission intensities.

Second, for determination of the photon emission intensities, three sources were simultaneously measured on three N-type high-purity germanium (HPGe) detectors: two 100 cm^3 coaxial HPGe detectors (G8 (diameter: 49.5 mm – thickness: 47.8 mm, with 500-µm thick beryllium window)) and G9 (diameter: 48.7 mm – thickness: 55.4 mm, with 500-µm thick beryllium window)) were used for the energy range, between 50 keV and 500 keV, with different geometrical conditions. The measurement with G9 was carried out in the efficiency calibration geometrical condition (source-detector distance of about 10 cm) and, for G8, the source was placed at about 2 cm from the detector window and a 2-mm thick copper absorber was interposed between these. This experimental condition was chosen in order to significantly reduce the counting rate due to low-energy photons and, consequently, to improve the detection limit for the low-intensity gamma-rays. In addition, the low-energy gamma- and K X-ray emissions were measured using a planar detector (GENIX (diameter: 12 mm – thickness: 6.7 mm, with 127-µm thick beryllium window, equipped with 2-mm thick tantalum collimators) in the calibration conditions, and a silicon drift detector (SDD (area: 25 mm^2 – thickness: 0.5 mm, with 12.5-µm thick beryllium window, equipped with a specific multi-element collimator reducing the active area to 17 mm^2)) was used to obtain information on the L X-ray emissions relative intensities.

Efficiency calibration

The full-energy peak efficiency calibration was established with standard point sources, prepared at LNHB, from radioactive solutions whose mass activity was determined with relative standard uncertainties lower than 0.5%. For each energy, E_i, the full-energy peak (FEP) efficiency, ε_i, is derived from the count rate in the relevant peak, n_i:

$$\varepsilon_i = \frac{n_i \cdot \prod C_{ij}}{A \cdot I_i} \qquad \textit{(Equation 1)}$$

A is the source activity (Bq) and I_i is the emission intensity of photons with energy E_i for the measured radionuclide. $C_{i,j}$ stands for different correction factors including radioactive decay and coincidence summing. The FEP net areas were obtained by using the COLEGRAM software which proposes different mathematical functions to fit the experimental points by the least-squares minimization method (Ruellan *et al.*, 1996).

For the large detectors (G8 and G9) the calibration source-to-detector distances are 106.9 mm and 102.7 mm, respectively; in these geometrical conditions, the coincidence summing effect, calculated with the ETNA software (Piton et *al.*, 2000), induces a maximum corrective factor of 1.03 for multi-gamma emitting radionuclides such as ^{152}Eu or ^{133}Ba. For the planar detector (GENIX), the calibration distance is 78.07 mm and the coincidence corrective factors are less than 1.005. In any case, the individual FEP efficiency experimental values are obtained with a relative standard uncertainty typically less than 0.5 % for the energy range above 100 keV and about 1 % for the lower energy range.

Depending on the calibration energy range, more than twenty standard radionuclides were measured, providing about 100 experimental data (energy, efficiency) for each of the two large HPGe detectors, and 40 for the planar one. These were fitted using a log-log polynomial function. Finally, the FEP efficiency calibration curves are obtained over the energy range from 15 keV to 200 keV or 1 836 keV, respectively for the planar or the coaxial detectors, with a relative combined standard uncertainty of about 0.5 % for the high energy range, and of 1–2% below 100 keV.

High energy range

The absolute emission intensities were derived from a spectrum acquired during 10^6 seconds live time (1 037 468 seconds real time for G9 (4.4 % to 2.9 % dead time, which remains below

the rate inducing pile-up distortion), and 1 000 404 seconds for G8 (0.05 % to 0.04 % dead time). This acquisition time was split into 10 steps, subsequent spectra being recorded at the end of each interval, and the consistency between these was checked in the same way as for the sources homogeneity control. The ten consecutive counting results exhibited a good homogeneity, which made it possible to sum the spectra to improve the detection limits. The resulting summed spectrum recorded in the energy range from 8 keV to 550 keV in the calibration conditions (detector G9) is presented in Figure 3 (blue line) where the summed spectrum recorded close to the detector window, with copper absorber (detector G8) is plotted in red. The peaks corresponding to ^{103}Pd decay are indicated in Figure 3, the other peaks being identified as background radiations (natural radioactive decay chains).

For each energy, E_i, the photon emission intensity, I_i, is derived from the net count rate in the relevant peak, n_i:

$$I_i = \frac{n_i \cdot \prod C_{ij}}{\varepsilon_i \cdot A} \qquad \textit{(Equation 2)}$$

ε_i is the FEP efficiency for this energy and the geometrical arrangement;

A is the source activity (Bq), and $C_{i,j}$ represents different correction factors.

The corrective factors for radioactive decay are 1.14 (decay from reference date) and 1.26 (decay during acquisition); the maximum correction for coincidence summing is 1.8 % for the reference position measurements and 3.9 % for the short distance measurement.

In addition, the change of geometrical conditions for the measurement at 2 cm (G8) requires to calculate a correction factor for efficiency transfer between the calibration geometry and the measurement one. The corrective factor, computed with ETNA, is about 5.5 for the high energy range and is consequently given a large relative uncertainty (10 %). The uncertainty budget associated with the 357.45 keV emission intensity calculation is given in Table 2. For the 39.748-keV emission, the main differences in the uncertainty budget are those due to statistics

and detection efficiency, respectively 0.09% and 1%, giving the relative combined uncertainty of 1.06%.

From the measurement at the calibration distance (G9), only the four major peaks at 62.41 keV, 294.98 keV, 357.45 keV and 497.080 keV could be quantified. The 62.41-keV peak appears in a doublet, with a peak at 63.3 keV due to background radiation from the ^{238}U decay chain, with about the same intensity. Figure 4 shows the example of the processing of the 60-keV energy region using COLEGRAM with the results of the fitting of two peaks using Gaussian functions to derive the peak area corresponding only to ^{103}Pd photon emission.

A correction representing 27 % of the net peak area for background counting (^{214}Pb) was applied to the peak at 294.98 keV. The last two peaks, with higher energies did not suffer from any interference and their net areas were obtained from fitting simple Gaussian functions.

Unfortunately, the measurement at short distance with the copper screen did not provide much more information: only two peaks with energies 317.72 keV and 443.79 keV could be quantified in addition to the more intense ones, however with a large statistical uncertainty (respectively about 7 % and 30 %). Finally, the combined standard uncertainties including the efficiency transfer contribution, are respectively about 12 % and 32 %. It was checked that the intensities obtained with the intense peaks agree within the associated uncertainties with those obtained in the calibration conditions.

Low-energy range

The spectrum obtained in the low-energy range, with the planar HPGe detector is presented in Figure 5. The gamma transition from the metastable level induces a low-energy gamma-ray emission, with energy 39.748 keV. As shown in Figure 6, the spectrum in this energy range includes the peak of interest and a small peak around 40.3 keV, induced by pile-up of the Kα X-rays. These were processed by COLEGRAM using two Gaussian functions which are fitted

to the experimental data, to derive the individual peak areas. In the lower energy range, the peaks due to K X-ray emissions are processed using Voigt functions to take account of the natural line width of X-rays, the corresponding Lorentzian width been taken from tabulated values (Campbell and Papp, 2001). The intensity of the four K X-ray components are derived with about 1.1 % relative combined standard uncertainty. The value obtained for the 62.41 keV, obtained with 2.5 % relative combined standard uncertainty, is in agreement with the one derived from the large detector (relative difference less than 1 % between the two results).

L X-ray relative emission intensities

Complementary measurements were performed using a silicon drift detector (SDD) to record the L X-ray emissions of Rh, around 2 keV, together with the K X-rays. The processing of the L lines is conducted as for the K X-rays, using Voigt functions with individual Lorentzian widths, as displayed in Figure 7.

The SDD full energy peak efficiency is computed as the product of the intrinsic efficiency for energy E, $\varepsilon_i(E)$, and the geometrical efficiency, ε_G. The first one is obtained as a simple calculation taking into account the geometrical parameters of the detector and escape effects:

$$\varepsilon_i(E) = T_{Be}(E) \cdot T_{Air}(E) \cdot T_{Mylar}(E) P_{Si}(E) \cdot C_{esc}(E) \qquad \textit{(Equation 3)}$$

where

$$T_i(E) = exp(-\mu_i(E) \cdot x_i) \quad \textit{(Equation 4)}$$

$T_{Be}(E)$, $T_{Air}(E)$ and $T_{Mylar}(E)$ are respectively the transmission through the beryllium window, the air gap between the source and the detector, and the Mylar® film supporting the radioactive deposit; x_i is the absorber thickness and $\mu_i(E)$ is the mass attenuation coefficient of the absorber material for the incident energy;

$P_{Si}(E)$ is the probability of absorption in the silicon detector with thickness x_{Si} :

$$P_{Si}(E) = 1 - exp(-\mu_{Si}(E) \cdot x_{Si}) \quad \textit{(Equation 5)}$$

where $\mu_{Si}(E)$ is the mass attenuation coefficient of silicon for the incident energy;

$C_{esc}(E)$ is the correction for escape of silicon K X-rays:

$$C_{esc}(E) = \frac{1}{1+Pesc(E)} \qquad \textit{(Equation 6)}$$

$P_{esc}(E)$ is the escape probability:

$$P_{esc}(E) = 0.5 \cdot \omega_K \cdot \left(1 - \frac{1}{r}\right) \cdot \left[1 - \frac{\mu_{Si}(E_K)}{\mu_{Si}(E)} \cdot ln\left(1 - \frac{\mu_{Si}(E)}{\mu_{Si}(E_K)}\right)\right] \qquad \textit{(Equation 7)}$$

where E_K is the energy of Si K X-rays (1.74 keV),

ω_K is the silicon fluorescence yield (0.05037),

and *r* is the jump factor, that is the ratio of silicon mass attenuation coefficients at the K edge (10.37).

The geometrical efficiency is determined using radioactive standard sources (^{55}Fe and ^{109}Cd) to determine the solid angle in the measurement geometrical conditions. The relative combined standard uncertainty for this efficiency calibration is around 5 %. The absolute intensity of L X-ray emissions are derived from the comparison with the K X-ray intensity recorded simultaneously, which gives 8.61 (43) %. The relative intensities normalized to the $L_{\alpha 1,2}$ line are quoted in Table 3.

4. Synthesis and discussion on the decay scheme

The absolute photon emission intensities from the decay of ^{103}Pd are presented in Table 4, where the results of the present experiment are compared with the tabulated data (LARA, 2019). These are slightly different from De Frenne (2009), but have the interest to provide absolute values and include both the gamma- and L- (without detail on individual

contributions) and K-ray emission intensities. A major concern in any evaluation work is the normalization procedure that is performed either on the 39.748-keV or the 357.45-keV emission intensity. In the present study, we selected the last one, in spite of its lower emission intensity; indeed this *a priori* drawback is compensated by the better efficiency calibration (reduction of the uncertainty by a factor of two) in this energy range.

The 357.45-keV photon emission intensity is 0.02486(17) per 100 disintegrations; this value agrees with the tabulated data (0.0246 (6)) and is obtained with improvement of the associated combined standard uncertainty by a factor of three. In addition, the emission intensities of four other gamma-rays (39.748 keV, 62.41 keV, 294.98 keV and 443.79 keV) are also derived with reduction of the uncertainties.

It appears that three gamma-ray emissions (62.41 keV, 294.99 keV and 497.080 keV) from the third, fourth and fifth excited levels obtained in the present experiment have higher intensities than the tabulated data (respectively about 40 %, 6 % and 7 %). Conversely, for the gamma-ray emission from the metastable level (39.748 keV), the present result is 7 % lower than the tabulated value. Besides, the L- and K-X-ray emission intensities are also weaker by around 10 % than the tabulated data. This would suggest that the intensity of the electron capture towards the first excited level would be weaker, while the stronger intensities of the gamma-ray emissions would indicate that the electron capture branches toward levels 3, 4 and 5 could be more intense. Another possibility would be a small electron capture branch (< 2 %) towards the ground state, which physically seems unlikely considering the first forbidden non-unique nature of this transition.

Table 5 presents the relative photon emission intensities, compared with some previous measurements: the emission intensity of the 357.45 keV gamma-ray is used as the reference, with 100 % relative intensity. Except for two lines, few experimental data are available and some values may be questionable. For example, the high values for the 62.41 keV emission

intensity as provided by Saraf (1955) and Grunditz (1969) could be overestimated because of the interference of the 63.3 keV gamma-ray from ^{238}U decay chain (see Figure 4). The same effect (presence of ^{214}Pb background radiation) may have incorrectly increased the reported intensities of the 294.98-keV peak. The emission intensity of the 39.748-keV may also have been affected by pile-up from K X-rays, which was difficult to assess in the old experiments with low energy resolution, contrarily to the spectra obtained in the present study (see *e.g.* Figure 5).

C**onclusion**

This paper reports the experiment conducted to determine the photon emission intensities in the decay of ^{103}Pd. Specific sources were prepared with a palladium solution which was standardized with a relative uncertainty of 0.26% by liquid scintillation, using the Triple-to-Double Coincidence Ratio method. Due to the reference activity photon spectrometry performed, with accurately calibrated detectors, the absolute photon emission intensities with improved uncertainties (by a factor of three for the most intense ones) compared to previously published values were obtained. However, due to the large dynamic of the emission intensities, the accurate measurement of the weak ones is difficult and the balance of the decay scheme of ^{103}Pd still requires further careful investigations that should be conducted in parallel with studies on ^{103m}Rh which can provide complementary information. In the frame of a study dedicated to ^{103m}Rh as a neutron dosimeter, Riffaud *et al*. (2018) measured the K X-ray emission intensities in the decay of ^{103m}Rh and Riffaud (2018) determined some atomic parameters of rhodium (mass attenuation coefficients and fluorescence yields) and provided preliminary information on the decay scheme of ^{103}Pd: the measured photon emission intensities of ^{103m}Rh allowed to derive the internal conversion coefficients of the 39.748-keV transition as 145 (5) and 1516 (28), respectively for K and total, which also questions the

multipolarity of this transition from the metastable state considered as E3 in De Frenne (2009). In addition, the recent results of Nica *et al.* (2018) also showed that the 39.748-keV transition is an E3+M4 mixture with δ=0.023(5). In the present results, some inconsistency between the 39.748-keV and the KX-ray emission intensities are also noted, which could not yet be fully understood, however the ratio of these emission intensities is compatible between our measurement (0.000910 (13)) and the tabulated data in LARA (0.000907 (46)). The calculated transition probability from the metastable state is (98.1 (21)) % using our gamma emission intensity and the total internal conversion coefficient given above, compared to 98 (5) % (De Frenne, 2009), which is not consistent with the electron capture feeding to this level (99.9 %), indicating that the decay scheme is in itself not well balanced. The results obtained in the present study provide new information and give some useful clues that can be exploited in new comprehensive evaluations of the decay schemes of both ^{103}Pd and ^{103m}Rh, which are clearly required.

References

Avignon, P., Michalowicz, A., Bouchez, R., 1955. Étude de la désintégration du ^{103}Pd. Le Journal de Physique et le Radium 16, 5, 404-410.

Avignone, F.T., Frey, G.D., 1971. Internal Conversion and γ–γ directional correlation studies in the decay of ^{103}Ru, Physical Review C 4, 3, 912-918.

Babulal Saraf, 1955. Energy Levels of Rh^{103} from the Decay of Pd^{103} and Ru^{103}, Physical Review 97, 3, 715-720.

Bazhenov, V.A., Bakhshi-Zade, V.A., Aristov, E.A., Sokolova, T.N., Lumpov, A.I., 1985. Determination of absolute photon emission intensities in palladium-103 decay, Measurement Techniques, 18, 12, 1110-1112.

Berlyand, T.P., Grigor'ev, E.I., Orlov, V.P., 2002. Measurement of the Relative Intensity of ^{103}Pd Photon Radiation, Measurement Techniques 45, 9, 974–977.

Broda, R., Cassette, P., Kossert, K., 2007. Radionuclide metrology using liquid scintillation counting. Metrologia 44, S36-S52.

Campbell, J. L., Papp, T., 2001. Widths of the atomic K-N7 levels. Atomic Data and Nuclear Data Tables 77, 1-556. https://doi.org/10.1006/adnd.2000.0848

Cassette, P., Vatin, R., 1992. Experimental evaluation of TDCR models for the 3 PM liquid scintillation counter, Nuclear Instruments and Methods in Physics Research Section A, Volume 312, Issues 1–2, 95-99.

Cassette, P., Bé, M.-M., Jaubert, F., Lépy, M.-C., 2004. Measurement of a ^{103}Pd solution using the TDCR method by LSC, Applied Radiation and Isotopes 60, 439-445

Czock, K.H., Haselberger, N., Reichel, F., Popa, S., 1975. Determination of the Half-Life of ^{103}Pd, International Journal of Applied Radiation and Isotopes 26, 782-784.

De Frenne D., 2009. Nuclear data Sheets for A = 103, Nuclear data Sheets 110, 2081-2256.

Grunditz, Y., Antman, S., Pettersson, H., Saraceno, M., 1969. Studies in the decay of ^{103}Pd, Nuclear Physics A133, 369-384.

JCGM 101, 2008. Evaluation of measurement data — Supplement 1 to the "Guide to the expression of uncertainty in measurement" — Propagation of distributions using a Monte Carlo method.

Kibédi, T., Burrows, T. W., Trzhaskovskaya, M. B., Nestor, C.W., 2005. BRICC Program Package, v 2.0. ANU-P/1684.

LARA, 2019. http://www.lnhb.fr/donnees-nucleaires/module-lara/

Lépy, M.-C., Pearce, A., Sima, O., 2015. Uncertainties in gamma-ray spectrometry, Metrologia 52, S123–S145. doi:10.1088/0026-1394/52/3/S123.

Lépy, M.-C., Brondeau, L., Bobin, C, Lourenço, V., Thiam, C., Bé, M.-M., 2016. Determination of X- and gamma-ray emission intensities in the decay of I-131, Applied Radiation and Isotopes, 109, 154-159.

Lépy, M.-C., Brondeau, L., Ménesguen, Y., Pierre, S., Riffaud, J., 2018. Consistency of photon emission intensities for efficiency calibration of gamma-ray spectrometers in the energy range from 20 keV to 80 keV, Applied Radiation and Isotopes 134, 131-136.

Lindner, M., I. Perlman, I., 1948. Neutron Deficient Isotopes of Rhodium and Palladium, Physical Review 73, 10, 1202-1203.

Lourenço, V., Bobin, C., 2015. Weighing uncertainties in quantitative source preparation for radionuclide metrology, Metrologia 52, S18–S29. doi:10.1088/0026-1394/52/3/S18.

Macias, E.S., Phelps, M.E., Sarantites, D.G., Meyer, R.A., 1976. Decay of 39-day ^{103}Ru and 17-day ^{103}Pd to the levels of ^{103}Rh, Physical Review C, 14, 2, 639-644.

Manthuruthil, J. C., Hennzecke, H. J., Cothern, C. R., 1968. Internal-conversion–electron study of the decay of Ru103, Physical Review 165, 4, 1365-1370.

Matthews, D. E., Pool, M. L., 1947. X-Ray Emission from Radioactive Ce, Pd, and Ca, Physical Review 72, 163-164.

Mei, J.Y., Huddelston, C.M. Mitchell, Allan C.G, 1950. The disintegration of Ruthenium 103 and Palladium 103, Physical Review 79, 3, 429-432

Newton, D., Toureau, A.E.R., Anderson, A.L., Meyer, R.A., 1978. Relative High-Energy Gamma- and X-Ray emissions following the decay of ^{103}Pd, International Journal of Applied Radiation and Isotopes 29, 188-189.

Nica, N., Hardy, J. C., Iacob, V .E., Horvat, V., Park, H. I., Werke, T. A., Glennon, K. J., Folden III, C. M., Sabla, V .I., Bryant, J. B., James, X. K., Trzhaskovskaya, M. B., 2018. Precise measurement of αK and αT for the 39.8-keV E3 transition in ^{103}Rh: Test of internal-conversion theory, Physical Review C 98, 054321, 1-11.

NORDION, 2019. https://www.nordion.com/

Panontin, J. A., Porile, N. T., Caretto, A. A. Jr, 1968. Nuclear reactions of Silver and Indium with 200- and 400-MeV protons, Physical Review 165, 4, 1273-1281.

Piton, F., Lépy, M.-C., Bé, M.-M., Plagnard, J., 2000. Efficiency transfer and coincidence summing corrections for gamma-ray spectrometry, Applied Radiation and Isotopes 52,791-795. doi: 10.1016/S0969-8043(99)00246-8

Popov, Yu. S., Zakharova, L.V., Kupriyanov, V.N., Andreev, O.I., Pakhomov, A.N., Vakhetov, F. Z., 2004. Half-Life and Photon Intensities of ^{103}Pd, Radiochemistry 46, 3, 209-210

Rietjens, L. H. Th., Van Den Bold, H. J., Endt, P. M., 1954. Continuous and discrete gamma-radiation in the decay of ^{103}Pd, Physica 20, 1, 107-114.

Riffaud, J., Cassette, P., Lacour, D., Lourenço, V., Tartès, I., Kellett, M.A., Corbel, M., Lépy, M.-C., Domergue, C., Destouches, C., Carcreff, H., Vigneaud, O., 2018. Measurement of absolute K X-ray emission intensities in the decay of ^{103m}Rh, Applied Radiation and Isotopes 134 (2018) 399-405.

Riffaud, J., 2018. Contribution à l'amélioration de la mesure absolue de l'activité de dosimètres émetteurs de rayons X irradiés en réacteur nucléaire. PhD Thesis, Université Paris-Saclay.

Ruellan, H., Lépy, M.-C., Etcheverry, M., Plagnard, J., Morel, J., 1996. A new spectra processing code applied to the analysis of ^{235}U and ^{238}U in the 60–200 keV energy range, Nuclear Instruments and Methods in Physics Research A369, 651-656.

Salvat, F., 2015. PENELOPE-2014: A code System for Monte Carlo Simulation of Electron and Photon Transport, OECD/NEA Data Bank, NEA/NSC/DOC(2015)3. Issy-les-Moulineaux, France. Available from ⟨http://www.nea.fr/lists/penelope.html⟩

Vaninbroukx, R., Grosse, G., Zehner, W., 1981. New determination of the half-lives of ^{57}Co, ^{103}Ru, ^{103m}Rh, ^{103}Pd and ^{109}Cd, International Journal of Applied Radiation and Isotopes 32, 589-591.

Zoller, W.H., Macias, E.S., Perkal, M.B., and Walters, W.B., 1969. Decay of 40-d ^{103}Ru and 17-d ^{103}Pd to levels of 103Rh, Nuclear Physics A130, 293-304. doi:10.1016/0375-9474(69)90731-3.

Figure captions:

Figure 1: ^{103}Pd decay scheme (De Frenne, 2009)

Figure 2: ^{103}Pd half-life measurement. Upper panel: net counting in the 357.45-keV peak (blue diamonds) versus the acquisition time with fitted exponential function (red curve) - Lower panel: relative residuals

Figure 3: Spectra of ^{103}Pd recorded with coaxial detectors in the 8 keV -550 keV energy range. Relative residuals are plotted in the lower panel.

Blue: Point source at 102.7 mm from G9 detector window (calibration condition)

Red: Point source at 26.9 mm from G8 detector window, with copper absorber

Figure 4: Fit of two Gaussian functions to the experimental data of the 62-63 keV doublet in the spectrum of ^{103}Pd (Detector G9- calibration position)

Figure 5: Spectrum of ^{103}Pd in the low-energy range recorded with detector GENIX

Figure 6: Fit of two Gaussian functions to the experimental data of the 39.748-keV doublet in the decay of ^{103}Pd (Detector GENIX)

Figure 7: Processing of the Rh L X-ray region recorded by SDD detector using Voigt functions

Table captions:

Table 1: Results of ^{103}Pd half-life measurements

Table 2: Uncertainty budget for the 357.45-keV emission intensity

Table 3: Relative intensities of the individual Rh L X-ray emissions in the decay of ^{103}Pd

Table 4: Absolute photon emission intensities in the decay of ^{103}Pd

Table 5: Relative photon emission intensities in the decay of ^{103}Pd (I_γ (357.45 keV) = 100 %)

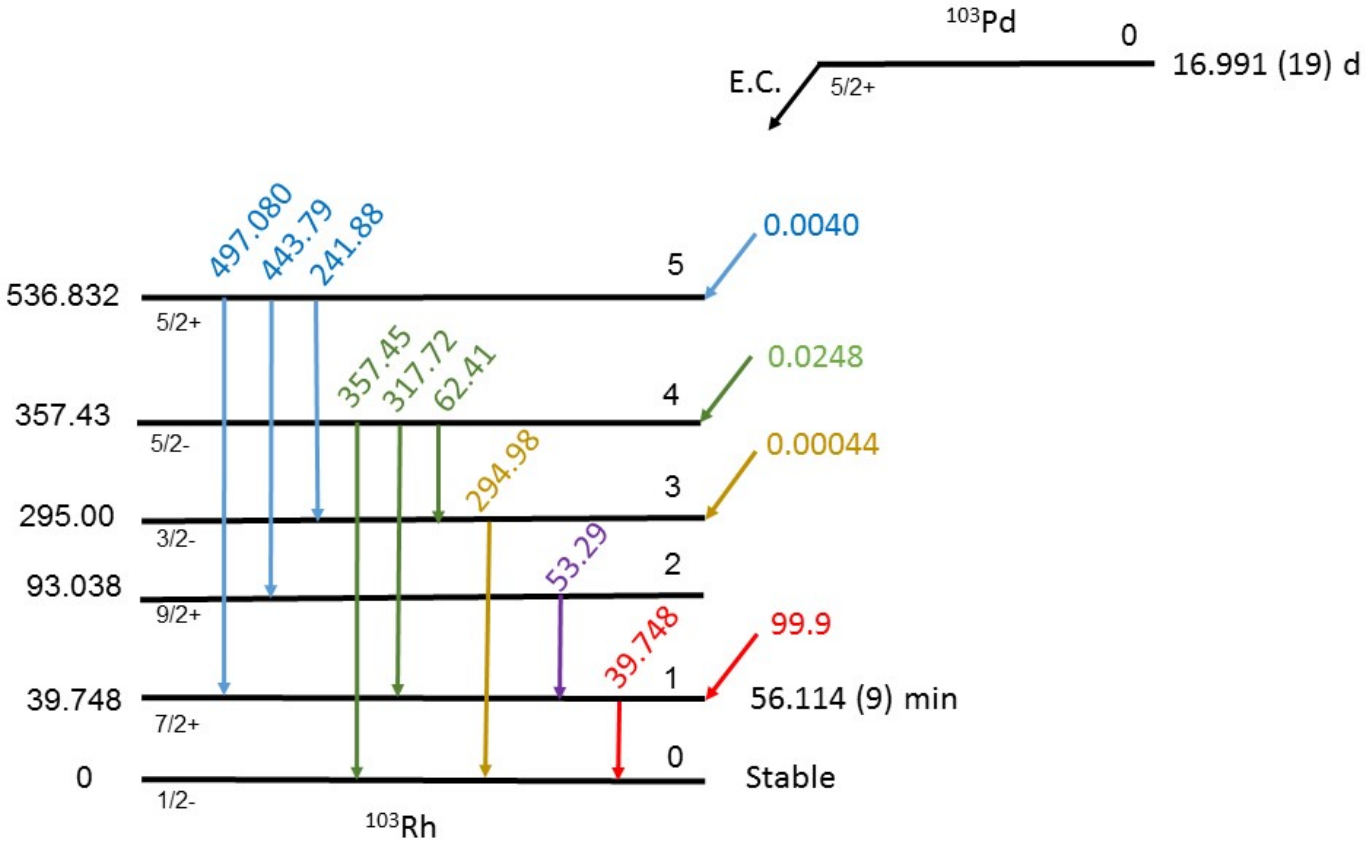

Figure 1: ^{103}Pd decay scheme (De Frenne, 2009)

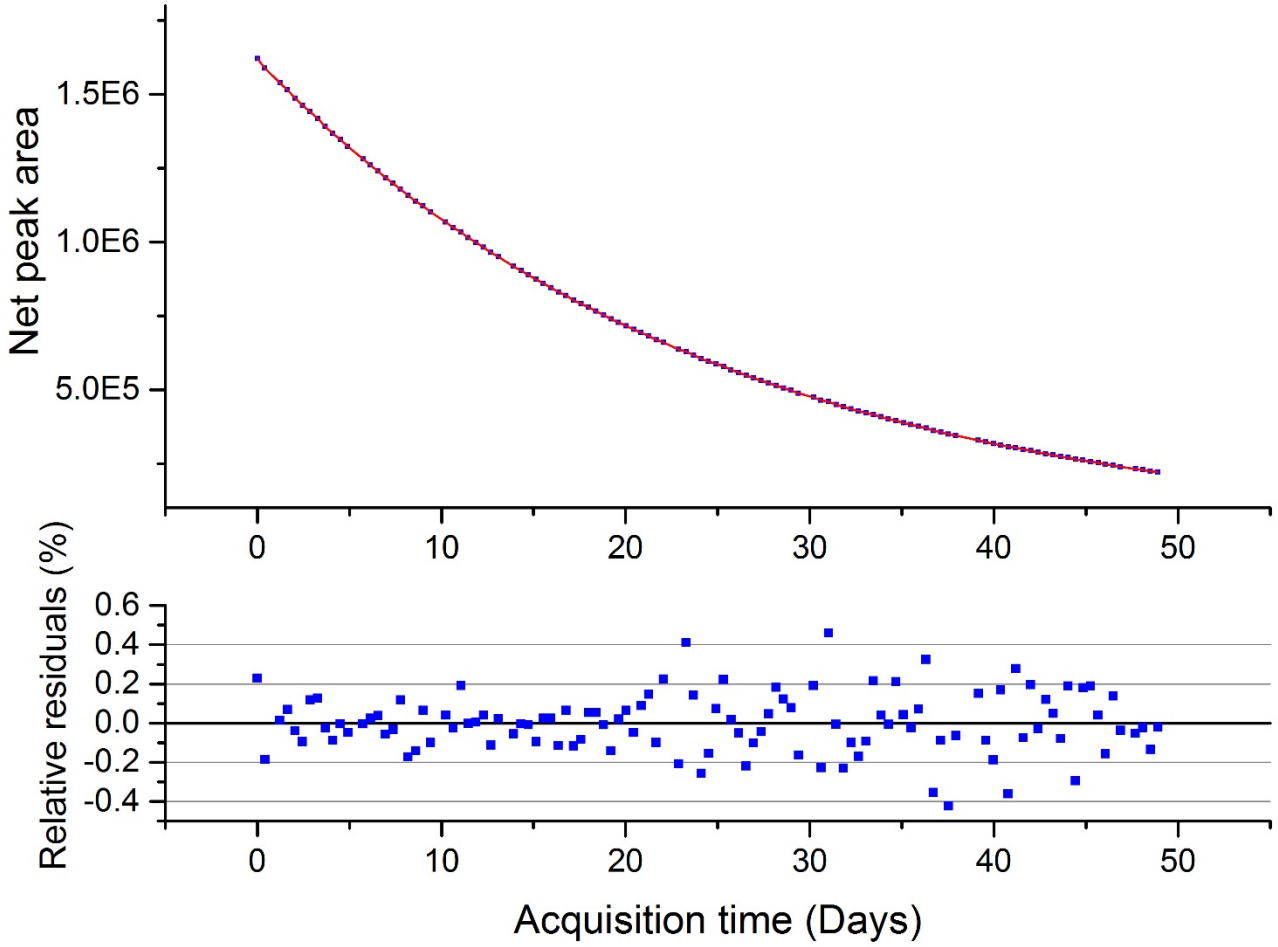

Figure 2: ^{103}Pd half-life measurement: upper panel: net counting in the 357.45-keV peak (blue diamonds) versus the acquisition time with fitted exponential function (red curve). Lower panel: relative residuals

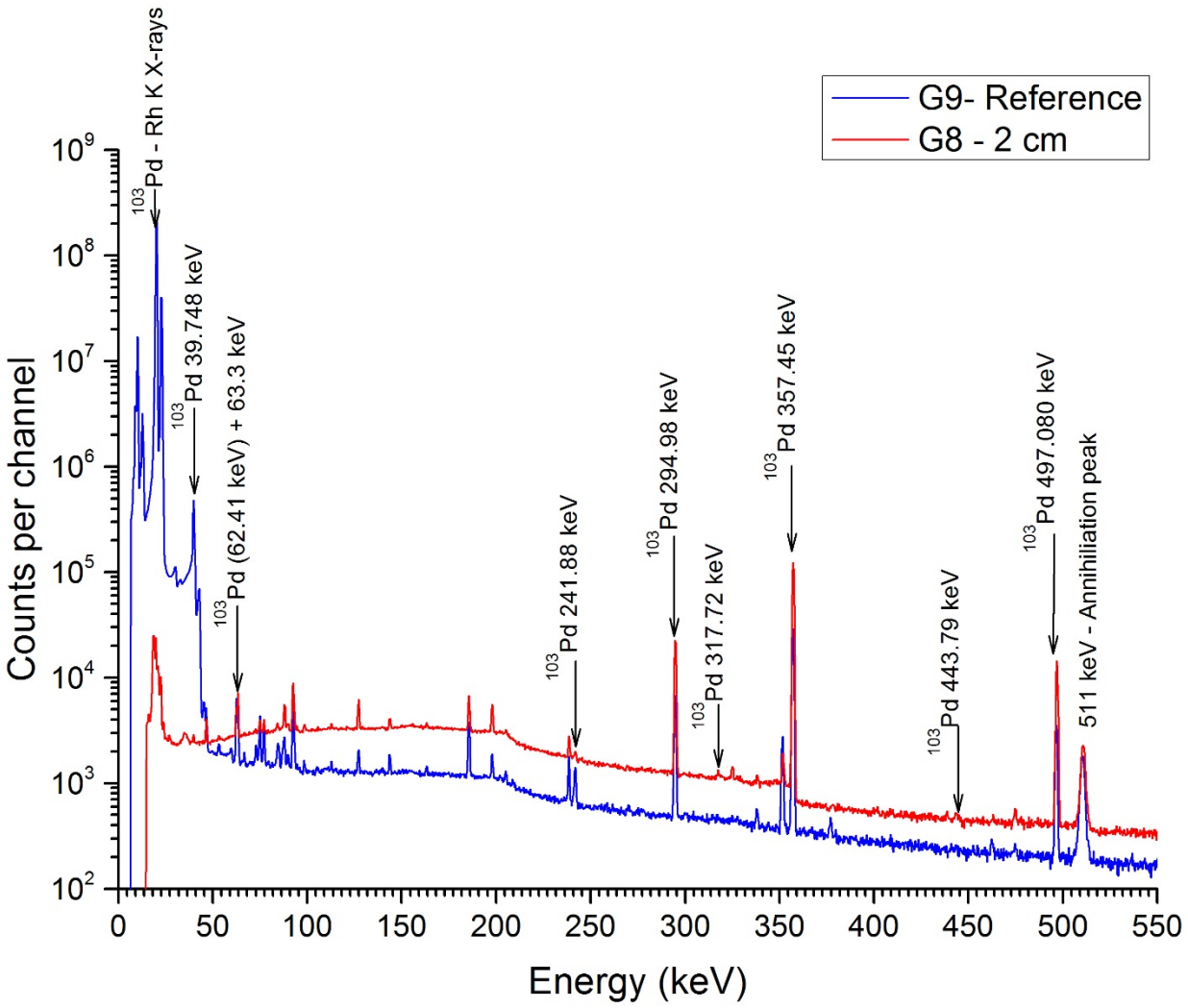

Figure 3: Spectra of ^{103}Pd recorded with coaxial detectors in the 8 keV -550 keV energy range.

Blue: Point source at 102.7 mm from G9 detector window (calibration condition)

Red: Point source at 26.9 mm from G8 detector window, with copper absorber

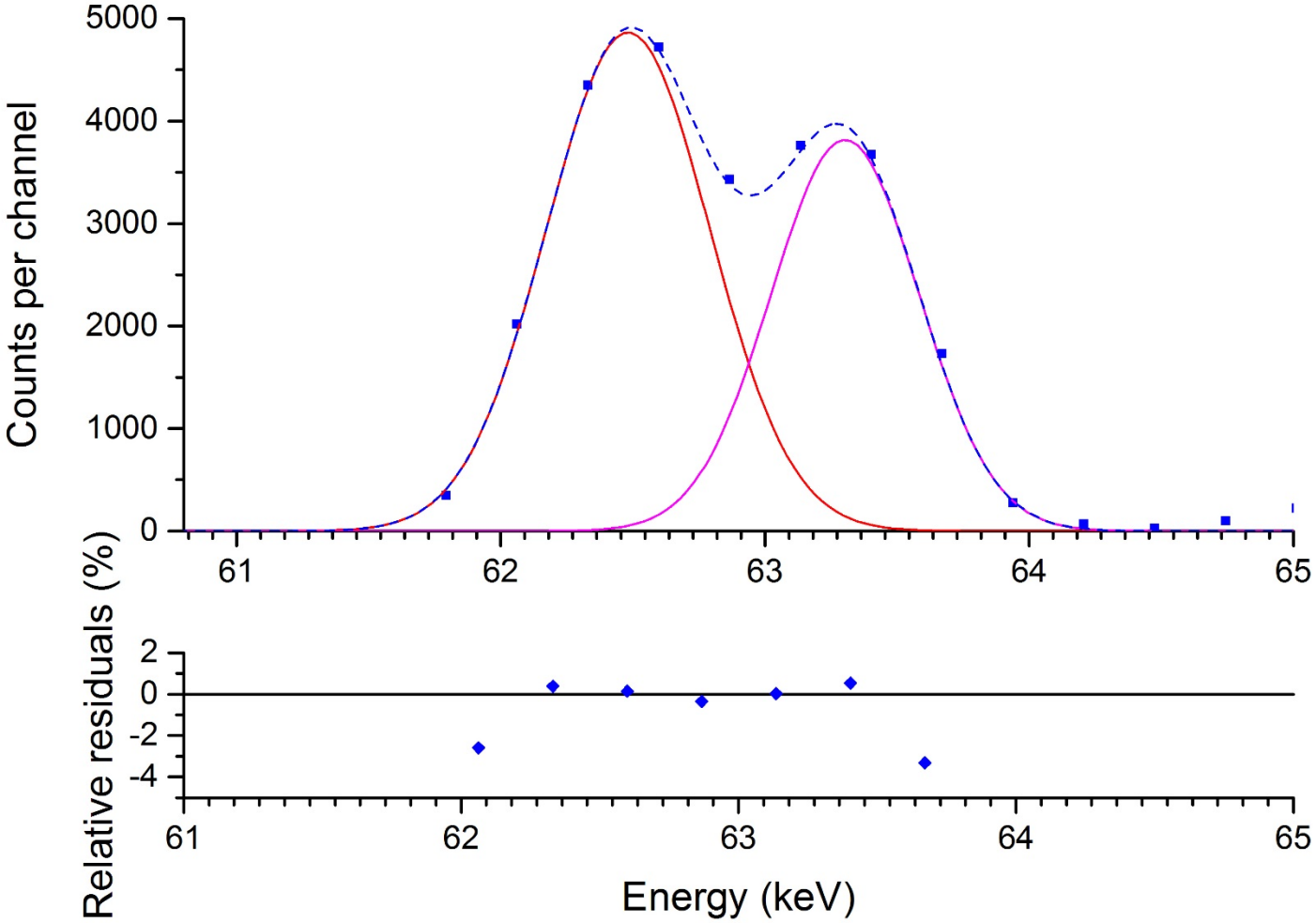
Counts per channel
5000
4000
3000
2000
1000
0
61
62
63
64
65
Relative residuals (%)
2
0
-2
-4
61
62
63
64
65
Energy (keV)

Figure 4: Fit of two Gaussian functions to the experimental data of the 62-63 keV doublet in the spectrum of ^{103}Pd (Detector G9- calibration position). Relative residuals are plotted in the lower panel

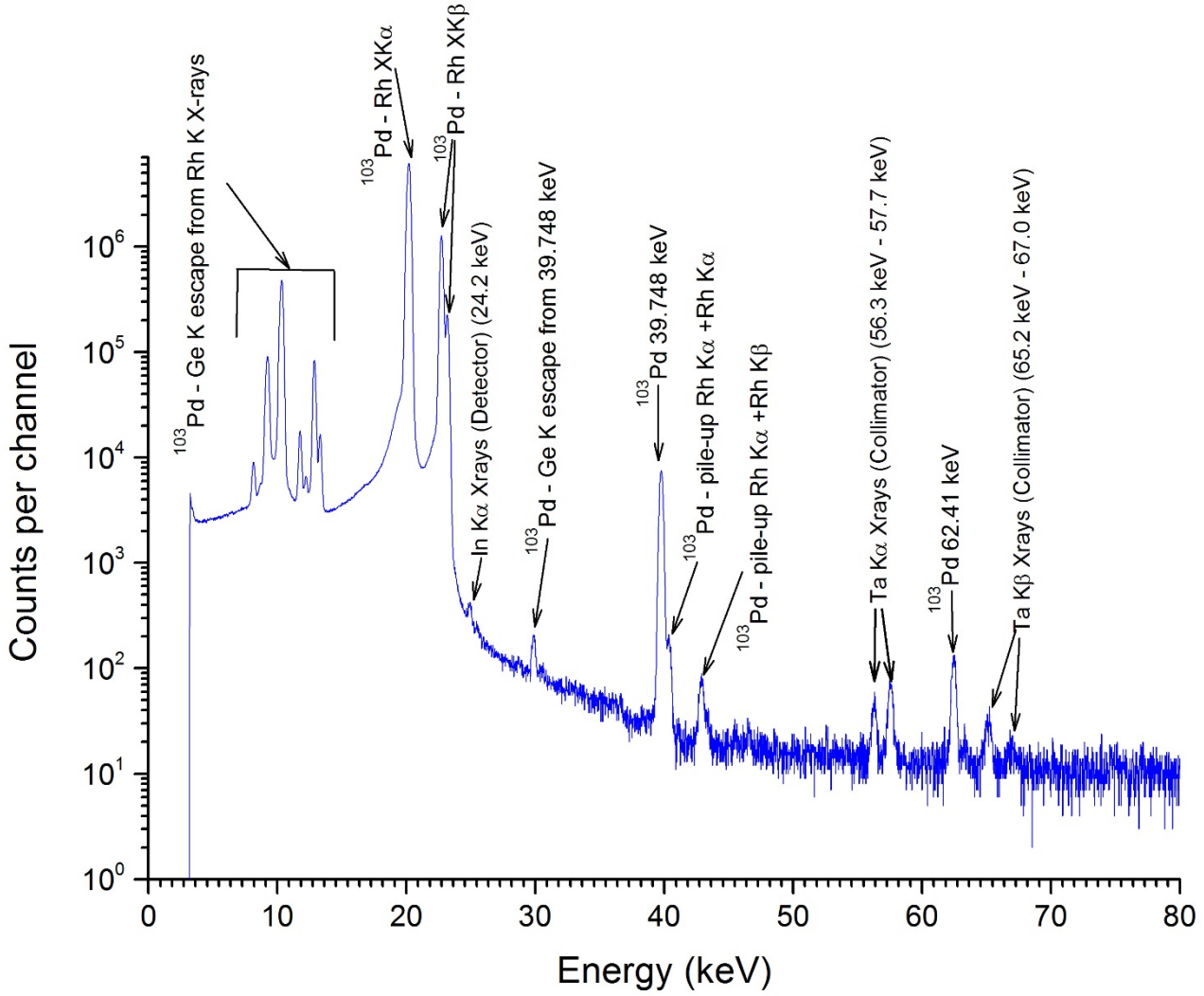

Figure 5: Spectrum of ^{103}Pd in the low-energy range recorded with detector GENIX

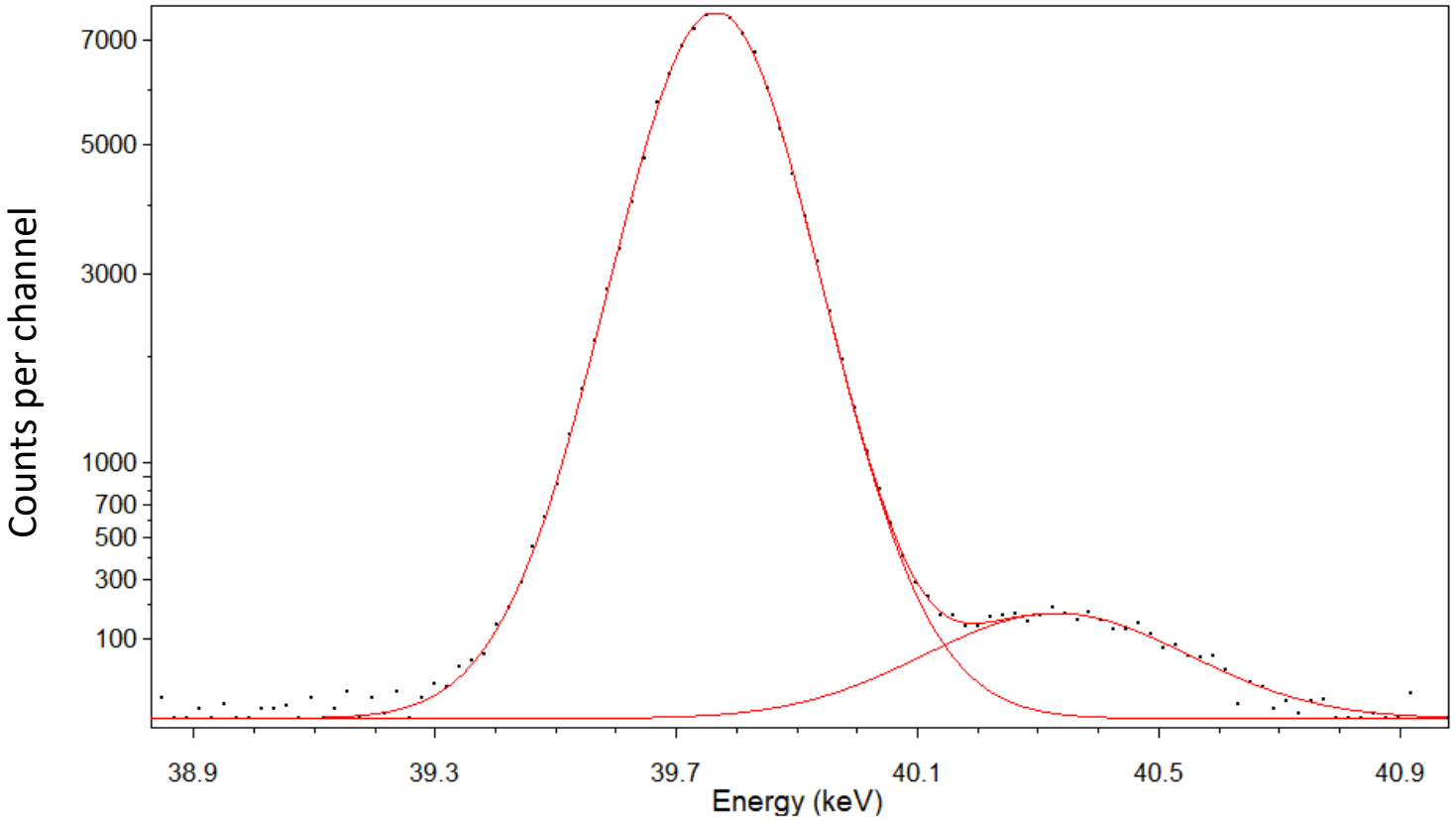

Figure 6: Fit of two Gaussian functions to the experimental data of the 62-63 keV doublet in the decay of ^{103}Pd (Detector GENIX)

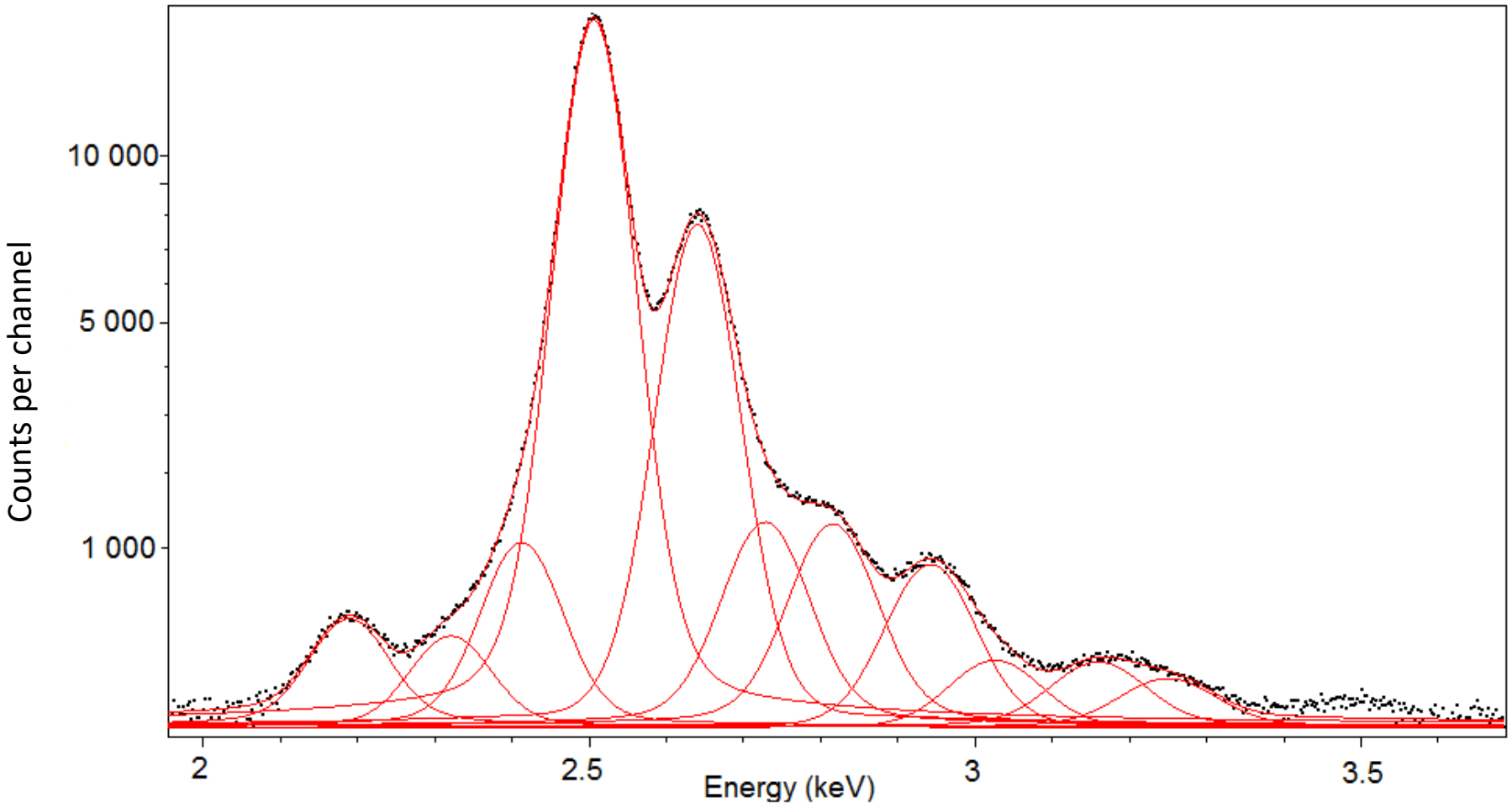

Figure 7: Processing of the Rh L X-ray region recorded by SDD detector, using Voigt functions

Authors	Year	Half-life (d)	Absolute uncertainty (d)	Relative uncertainty (%)	Number of half-lives
Rietjens et al.	1954	17.5	0.5	2.86	
Panontin et a.	1968	16.9	0.1	0.59	
Grunditz et al.	1969	18.4	0.5	2.72	4
Czock et al.	1975	16.961	0.016	0.09	2
Vaninbroukx et al.	1981	16.991	0.019	0.11	2-3
Popov et al.	2004	16.8	0.6	3.57	5.9
Present study	**2017**	**17.049**	**0.016**	**0.09**	**2.9**

Table 1: Results of ^{103}Pd half-life measurements

Individual components	Calibration conditions	With efficiency transfer
	$u(I_\gamma)/I_\gamma$ (%)	$u(I_\gamma)/I_\gamma$ (%)
Statistical uncertainty	0.31	0.08
Activity	0.25	0.25
Full-energy peak detection efficiency	0.5	0.5
Full-energy peak area (fitting)	0.2	0.2
Decay correction (reference)	0.008	0.008
Decay correction (during counting)	0.013	0.013
Coincidence summing	0.07	0
Efficiency transfer	0	10.0
Weighing	0.022	0.027
Combined uncertainty	**0.68**	**10.02**

Table 2: Uncertainty budget for the 357.45-keV emission intensity

Line	Levels	Energy (keV)	Relative intensity
Ll	L3-M1	2.370	2.67 (14)
Lη	L2-M1	2.513	1.73 (9)
Lα1,2	L3-M4,5	2.695	100 (5)
Lβ1	L2-M4	2.891	48.5 (24)
Lβ4	L1-M2	2.891	8.23 (41)
Lβ3	L1-M3	2.915	
Lβ6	L3-N1	2.934	
Lβ2,15	L3-N4,5	3.012	8.00 (40)
Lβ9,10	L1-M4,5	3.101	4.94 (25)
Lγ1	L2-N4	3.154	0.841 (43)
Lγ2,3	L1-N2,3	3.373	0.848 (44)

Table 3: Relative intensities of the individual Rh L X-ray emissions in the decay of ^{103}Pd

	LARA (2019)		Present study	
Energy (keV)	**Photon emission intensity (%)**	**Relative uncertainty (%)**	**Photon emission intensity (%)**	**Relative uncertainty (%)**
XL	8.73 (23)	2.6	8.61 (43)	5
20.07 (Kα2)	22.05 (22)	1.0	19.59 (21)	1.1
20.22 (Kα1)	41.70 (40)	1.0	39.48 (42)	1.1
K alpha total	63.75 (46)	0.7	59.07 (47)	0.8
22.81 (Kβ1)	11.34 (15)	1.3	10.27 (11)	1.1
23.20 (Kβ2)	1.88 (7)	3.7	1.781 (19)	1.1
K beta total	13.22 (17)	1.3	12.05 (11)	0.9
K total	76.97 (49)	0.6	71.1 (6)	0.9
39.748	0.0698 (35)	5	0.0647 (7)	1.1
53.29	7.2 (20) 10^{-6}	28	< 8 10^{-6}	-
62.41	7.8 (23) 10^{-4}	29	0.001128 (16)	1.4
241.88	4.9 (5) 10^{-7}	10	-	-
294.98	0.00297 (24)	8	0.00315 (7)	2.3
317.72	1.50 (19) 10^{-5}	13	1.37 (17) 10^{-5}	12.5
357.45	0.0246 (6)	2.4	0.02486 (17)	0.68
443.79	1.60 (12)10^{-5}	7.5	2.1 (8) 10^{-5}	32.5
497.08	0.00411 (11)	2.7	0.00439 (7)	1.6

Table 4: Absolute photon emission intensities in the decay of ^{103}Pd

Energy (keV)	Rietjens et al. (1954)	Avignon et al. (1955)	Saraf (1955)	Grunditz et al. (1969)	Zoller et al. (1969)	Macias et al. (1976)	Berlyand et al. (2002)	Popov et al. (2004)	Present study
39.748		1.00 (21)		1.38 (13)	2.11 (12)	3.10 (10)			**2.602 (28)**
62.41		0.089 (22)	0.061 (18)	0.069 (7)	0.0240 (22)	0.0471 (21)			**0.0454 (6)**
294.98	0.18 (5)	0.143 (31)	0.182 (41)	0.177 (25)	0.142 (15)	0.127 (5)	0.141 (35)	0.1230 (40)	**0.1268 (29)**
317.72					4.0 (10) 10^{-4}	6.81 (37) 10^{-4}			**5.5 (7) 10^{-4}**
443.79					7.5 (8) 10^{-4}	6.81 (37) 10^{-4}			**8.6 (28) 10^{-4}**
497.08	0.183 (40)	0.214 (47)	0.152 (23)	0.23 (11)	0.175 (19)	0.180 (8)	0.182 (36)	0.176 (6)	**0.1768 (28)**

Table 5: Relative photon emission intensities in the decay of ^{103}Pd ($I\gamma$ (357.45 keV) =100%)